

# MTGFlow: Unsupervised Multivariate Time Series Anomaly Detection via Dynamic Graph and Entity-aware Normalizing Flow

Qihang Zhou  
Zhejiang University

Jiming Chen  
Zhejiang University

Haoyu Liu  
Zhejiang University

Shibo He  
Zhejiang University

Wenchao Meng  
Zhejiang University

## ABSTRACT

Multivariate time series anomaly detection has been extensively studied under the semi-supervised setting, where a training dataset with all normal instances is required. However, preparing such a dataset is very laborious since each single data instance should be fully guaranteed to be normal. It is, therefore, desired to explore multivariate time series anomaly detection methods based on the dataset without any label knowledge. In this paper, we propose MTGFlow, an unsupervised anomaly detection approach for Multivariate Time series anomaly detection via dynamic Graph and entity-aware normalizing Flow, leaning only on a widely accepted hypothesis that abnormal instances exhibit sparse densities than the normal. However, the complex interdependencies among entities and the diverse inherent characteristics of each entity pose significant challenges on the density estimation, let alone to detect anomalies based on the estimated possibility distribution. To tackle these problems, we propose to learn the mutual and dynamic relations among entities via a graph structure learning model, which helps to model accurate distribution of multivariate time series. Moreover, taking account of distinct characteristics of the individual entities, an entity-aware normalizing flow is developed to describe each entity into a parameterized normal distribution, thereby producing fine-grained density estimation. Incorporating these two strategies, MTGFlow achieves superior anomaly detection performance. Experiments on the real-world datasets are conducted, demonstrating that MTGFlow outperforms the state-of-the-art (SOTA) by 5.0% and 1.6% AUROC for SWaT and WADI datasets respectively. Also, through the anomaly scores contributed by individual entities, MTGFlow can provide explanation information for the detection results.

## CCS CONCEPTS

• Computing methodologies → Anomaly detection; • Theory of computation → Unsupervised learning and clustering.

## KEYWORDS

multivariate time series, anomaly detection, normalizing flow, graph structure learning

## 1 INTRODUCTION

Multivariate time series broadly exist in many important scenarios, such as production data produced by multiple devices in smart factories and monitoring data generated by various sensors in smart grids. Anomalies in multivariate time series exhibit unusual data behaviours at a specific time step or during a time period. To identify

these anomalies, previous methods mostly focus on training one class classification (OCC) models from only normal data [2, 3, 5, 6, 25–28, 32]. They heavily rely on an assumption that the training dataset with all normal samples can be easily obtained.

However, this assumption may not always hold in real-world scenarios [9, 34, 35], leading to noisy training datasets with the mixture of normal and abnormal data instances. Meanwhile, it is already verified that model training procedure is prone to overfitting noisy labels [33], so that the performance of those OCC based methods could be severely degraded. Therefore, it is rewarding to develop unsupervised multivariate time series anomaly detection methods based on the dataset with absolute zero known labels.

An effective unsupervised strategy is modeling the dataset into a distribution, relying only on a widely accepted hypothesis that abnormal instances exhibit sparse densities than the normal, i.e., the low density regions consist of abnormal samples and the high density regions are formed by the normal samples [12, 17, 31]. Methods have been explored along side this strategy and the key challenge lies in the accurate density estimation of the distribution. Time series density is modeled as the parametrized probability distribution in DeepAR [24], while it is challenging to model a more complex data distribution. To improve model competence of density estimation, Rasul *et al.* [19] further exploits normalizing flow to model complex distribution for high-dimensional multivariate time series [19]. However, they neglect the interdependencies among constituent series which plays an equally important role for the accurate density estimation.

The most related work is GANF, which tackles the same multivariate time series anomaly detection task [5]. In their design, the static directed acyclic graph (DAG) is leveraged to model intractable dependence among multiple entities, and normalizing flow [7, 18] is employed to estimate an overall distribution for all entities together. Although GANF has achieved SOTA results previously, it still suffers from two drawbacks. First, in real-world applications, entities could have complex and evolving mutual dependence. For example, in a water treatment plant, when the measured motorized valve is on, water level will rise. While water level exceeds the necessity, the measured motorized valve will be closed. The actuator of the motorized valve and the water level sensor for the same water tank actually have strong coupling relations, which can not be simply characterized by a DAG structure. Meanwhile, due to different work conditions, the water level needs to rise for storing water or fall when draining water. Such relationships are not set in stone, and thus the static graph structure fails to have a comprehensive modeling capacity on this evolving feature. Second,

each entity may have different working mechanisms. This leads to the diverse sparse characteristics of the anomalies for different entities. GANF projects these various sparse characteristics into one distribution, resulting in a compromise for the density estimation of each individual time series. Thereby, the final anomaly detection performance could also be degraded.

In this paper, we propose MTGFlow, an unsupervised anomaly detection method for multivariate time series anomaly detection, to tackle the above problems. First, considering the evolving relations among entities, we introduce a graph structure learning module to model these changeable interdependencies. To learn the dynamic structure, a self-attention module [29] is plugged into our model because of its superior performance on quantifying pairwise interaction. Second, aiming at the diverse inherent characteristics existed among individual entities, we design an entity-aware normalizing flow to model the entity-specific density estimation. For this purpose, we assign each entity to a unique target distribution. As a consequence, diverse entity densities can be estimated independently, thereby mitigating the performance compromise of simultaneous estimation of multiple entities. However, this fine-grained density estimation of MTGFlow multiplies memory overhead as the number of entities increases. We share entity-specific model parameters to reduce model size. As a result, MTGFlow achieves more fine-grained density estimation without extra memory consumption, which further promotes the anomaly detection performance.

Finally, maximum likelihood estimation is used to train all parameters of MTGFlow in an end-to-end manner. Experiments are conducted on two real-world datasets SWaT and WADI to demonstrate the effectiveness of MTGFlow. MTGFlow makes progress over the SOTA, achieving 84.8% AUROC on SWaT and 91.9% AUROC on WADI, outperforming 5.0% and 1.6% than GANF, respectively. What's more, MTGFlow can interpret a detected anomaly via the log likelihood factors that each entity contributes. Through the learned graph structure, various dependence among individual entities can be represented. We summarize our contributions as follows:

- We propose MTGFlow, an approach for unsupervised multivariate time series anomaly detection, with the ability of result explanation and the anomaly localization.
- We model complicated interdependencies among entities as the dynamic graph. Through the learned dynamic graph structure, various mutual relations like evolving and periodic interdependencies can be captured among the individual entities.
- Aiming at different sparse characteristics existed in the individual entities, entity-aware normalizing flow is introduced to produce entity-specific density estimation.
- MTGFlow outperforms SOTA method GANF on public datasets SWaT and WADI, outperforming 5.0% AUROC on SWaT, 1.6% AUROC on WADI.

## 2 RELATED WORK

### 2.1 Time Series Anomaly Detection

Anomaly detection for time series is a classical research topic, which has been extensively investigated under OCC setting. Temporal

correlation is one of the most important feature of time series. Compared with the normal, anomalous time points and sequences often present unusual temporal correlations. To model the distribution of normal time series, DeepSVDD [21] maps training data into preset hypersphere, assuming that anomalous data lie outside this space during the test. EncDecAD [16] leverages LSTM [13] to extract sequence features, and designs the reconstruction task to detect anomalies. USAD [2] and DAEMON [3] use adversarial learning to promote reconstruction quality. Considering the much more complex temporal dependence of multivariate time series, Omni-Anomaly [26] constructs informative stochastic representations for a more robust performance. More recent works [32] and [28] utilize Transformer [29] for anomaly detection, leaning on the superiority modeling capacity of the self-attention mechanism for long-range relations. However, all these works are based on the assumption that training data are all normal. Existence of abnormal time series in the training dataset could severely degrade the performance of these OCC based detection methods. Therefore, instead of fitting distribution of normal training dataset, MTGFlow estimates density of unlabelled training dataset, and detects anomalies depending on their inherent low density characteristics.

### 2.2 Graph Structure Learning

Given a structured data, graph convolution networks (GCN) [15] and graph attention networks (GAT) [30] achieve great success in modeling their intrinsic patterns. In real scenarios, the graph structure is hardly to obtain in advance. Therefore, it is important to learn the underlying graph structure. GDN [6] learns a directed graph via node embedding vectors. According to the cosine similarity of embedding vectors, top-K candidates of each node are considered to have interdependencies on the node itself. GANF [5] models relations among multiple sensors, using DAG, and learns the structure of the DAG through continuous optimization with a simplified constraint that facilitates backward propagation. Our work MTGFlow models the mutual complex dependence as a fully connect graph via self-attention mechanism, so that a much more flexible relation among entities can be represented.

### 2.3 Normalizing Flow for Anomaly Detection

Normalizing flow is an important technology on density estimation and has been successfully utilized in image generation task [7, 18]. Recently, normalizing flow is also explored for anomaly detection based on the assumption that anomalies are in low density regions. DifferNet [20] and CFLOW-AD [11] leverage normalizing flow to estimate likelihoods of normal embeddings extracted by an encoder. They declare image defects when the embedding is far away from the dense region. The more relevant work GANF models relationships among constituent series via DAG, and uses graph-augmented flow model to estimate densities of multiple time series. GANF makes a breakthrough for unsupervised anomaly detection on multivariate time series. However, in GANF, DAG fails to model mutual dependence existing among entities, and different entities with diverse patterns are all mapped into one distribution. Instead, we construct a fully connected graph to model such intractable temporal dependence. Meanwhile, we use entity-aware normalizing flow to have a much more precise estimation of the density.

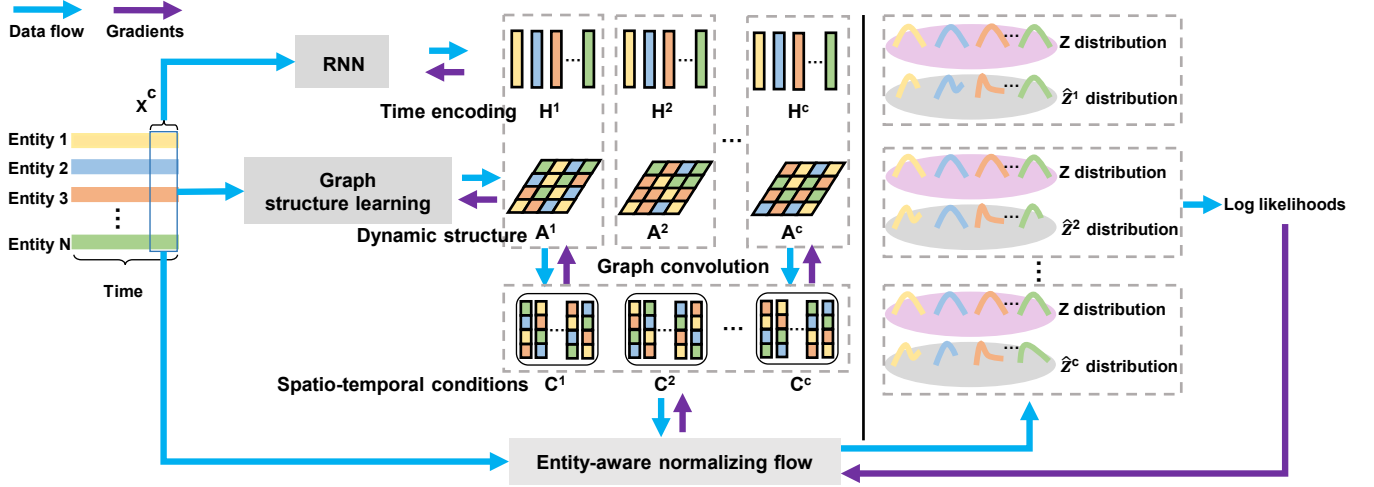


Figure 1: Overview of the proposed MTGFlow. Within a sliding window of size  $T$ , time series data  $x^c$  is fed to the RNN module to capture the temporal correlations. Hidden states of RNN are regarded as time encoding,  $H^c$ . Meanwhile,  $x^c$  is also input to the graph structure learning module to capture dynamic interdependencies among entities, which are modeled as adjacency matrix  $A^c$ . The spatio-temporal conditions  $C^c$  are derived via the graph convolution operation for  $H^c$  and  $A^c$ . Finally,  $C^c$  are used to help entity-aware normalizing flow model to produce entity-specific density estimation for the distribution of time series.

### 3 PRELIMINARY

In this section, we give a brief introduction of the self-attention mechanism and normalizing flow.

#### 3.1 Self-Attention

Transformer [29] has achieved great success for natural language processing (NLP), which largely benefits from the superior modeling capacity of the self-attention mechanism. For an input sequence,  $X = (x_1, x_2, x_3, \dots, x_N)$ ,  $x_i \in \mathcal{R}^D$ , where  $N$  is the sequence length, and  $D$  is the embedding dimension. Self-attention applies linear projections to get queries  $Q \in \mathcal{R}^{N \times D}$  and keys  $K \in \mathcal{R}^{N \times D}$  via learnable parameter matrices  $W^Q$ ,  $W^K$ . After projections, attention scores are derived by scaled dot product between  $Q$  and  $K$ , and a Softmax function is utilized to normalize the scores to  $(0,1)$ .

$$Q = XW^Q \quad \text{and} \quad K = XW^K$$

$$\text{Attention\_matrix} = \text{Softmax}\left(\frac{QK^T}{\sqrt{D}}\right) \quad (1)$$

With such a design, the pairwise relationships can be flexibly modeled in the neural network architecture. The obtained Attention matrix is the quantification of these relations.

#### 3.2 Normalizing Flow

Normalizing flow is an unsupervised density estimation approach to map original distribution to an arbitrary target distribution by the stack of invertible affine transformations. When density estimation on original data distribution  $\mathcal{X}$  is intractable, an alternative option is to estimate  $z$  density on target distribution  $\mathcal{Z}$ . Specifically, suppose a source sample  $x \in \mathcal{R}^D \sim \mathcal{X}$  and a target distribution sample  $z \in \mathcal{R}^D \sim \mathcal{Z}$ . Bijective invertible transformation  $\mathcal{F}_\theta$  aims to achieve

one-to-one mapping  $z = f_\theta(x)$  from  $\mathcal{X}$  to  $\mathcal{Z}$ . According to the change of variable formula, we can get

$$P_{\mathcal{X}}(x) = P_{\mathcal{Z}}(z) \left| \det \frac{\partial f_\theta}{\partial x^T} \right| \quad (2)$$

Benefiting from the invertibility of mapping functions and tractable jacobian determinants  $\left| \det \frac{\partial f_\theta}{\partial x^T} \right|$ . The objective of flow models is to achieve  $\hat{z} = z$ , where  $\hat{z} = f_\theta(x)$ . Parameters  $\theta$  of  $f_\theta$  can be directly estimated by maximum log likelihood as follows

$$\begin{aligned} \theta^* &= \arg \max_{\theta} (\log(P_{\mathcal{X}}(x))) \\ &= \arg \max_{\theta} (\log(P_{\mathcal{Z}}(f_\theta(x))) + \log\left(\left| \det \frac{\partial f_\theta}{\partial x^T} \right|\right)). \end{aligned} \quad (3)$$

Design of  $f_\theta$  is an important topic in flow models. The core is to improve the flow model transferability under the premise of the tractable jacobian determinants. Representative flow model like RealNVP [7] utilizes the affine coupling, while MAF [18] applies autoregressive functions.

Flow models are able to achieve more superior density estimation performance when additional conditions  $C$  are input [1]. This is because  $C$  can usually provide relevant priors to accurately characterize the source distribution, such as time and position encoding [29]. Such the flow model is called conditional normalizing flow, and its corresponding mapping is derived as  $z = f_\theta(x|C)$ . Therefore, the training objective is rewritten as

$$\theta^* = \arg \max_{\theta} (\log(P_{\mathcal{Z}}(f_\theta(x|C))) + \log\left(\left| \det \frac{\partial f_\theta}{\partial x^T} \right|\right)). \quad (4)$$

## 4 METHOD

### 4.1 Data Preparation

Multivariate time series are defined as  $x = (x_1, x_2, \dots, x_K)$  and  $x_i \in \mathcal{R}^L$ , where  $K$  represents the number of entities, and  $L$  denotes the total number of observations. We use the z-score to normalize the time series from different entities.

$$\bar{x}_i = \frac{x_i - \text{mean}(x_i)}{\text{std}(x_i)} \quad (5)$$

where  $\text{mean}(x_i)$  and  $\text{std}(x_i)$  represent the mean and standard deviation of  $i$ th entity along the time dimension, respectively.

To preserve the temporal correlation of the original series, we use a sliding window with size  $T$  and stride size  $S$  to sample the normalized multivariate time series.  $T$  and  $S$  can be adjusted to obtain the training sample  $x^c$ , where  $c$  is the sampling count. For better clarification, we notate the  $x^{cS:cS+T}$  as  $x^c$ .

### 4.2 Overall Structure

The core idea behind MTGFlow is to dynamically model mutual dependence so that fine-grained density estimation of the multivariate time series can be obtained. Such accurate estimations enable the superiority of capturing low density regions, and further promote the anomaly detection performance even if there is high anomaly contamination in training dataset. Fig. 1 shows the overview of MTGFlow. In particular, we model the temporal variations of each entity, using RNN model. Meanwhile, a graph structure learning module is leveraged to model the dynamic interdependencies. Then, the derived time encoding, output of RNN, performs graph convolution operation with above learned graph structure. We regard above outputs as spatio-temporal *conditions* as they contain temporal and structural information. Next, the spatio-temporal conditions are input to help entity-aware normalizing flow achieve precise fine-grained density estimation. The deviations of  $\hat{z}$  and  $z$  are measured by log likelihoods. Finally, all modules of MTGFlow are jointly optimized through maximum likelihood estimation.

### 4.3 Graph Structure Learning via Self-attention

Since dependence among entities is mutual and evolve over time, we exploit self-attention to learn a dynamic graph structure. Entities in multivariate time series are regarded as graph nodes. Given window sequence  $x^c$ , the query and key of node  $i$  are represented by vectors  $x_i^c W^Q$  and  $x_i^c W^K$ , where  $W^Q \in \mathcal{R}^{T \times T}$  and  $W^K \in \mathcal{R}^{T \times T}$  are the query weights and the key weights. According to Eq. 1, the pairwise relationship  $e_{ij}^c$  at the  $c$ th sampling count between node  $i$  and node  $j$  is described as

$$e_{ij}^c = \frac{(x_i^c W^Q)(x_j^c W^K)^T}{\sqrt{T}} \quad (6)$$

Attention score  $a_{ij}^c$  is used to quantify the pairwise relation from node  $i$  to node  $j$ , calculated by

$$a_{ij}^c = \frac{\exp(e_{ij}^c)}{\sum_{j=1}^n \exp(e_{ij}^c)} \quad (7)$$

Attention matrix combines attention scores of each node, thus including mutual dependence among entities. Naturally, we treat

attention matrix as the adjacency matrix  $A^c$ , which is represent by

$$A^c = \begin{bmatrix} a_{11}^c & \cdots & a_{1N}^c \\ \vdots & \ddots & \vdots \\ a_{N1}^c & \cdots & a_{NN}^c \end{bmatrix} \quad (8)$$

Since input time series are evolving over time,  $A^c$  also changes to capture the dynamic interdependencies.

### 4.4 Spatio-temporal Condition

To better estimate the density of multiple time series, the robust spatio-temporal condition information is important. As described in Sec. 4.3, underlying structure information is modeled as the dynamic graph. Besides spatio information, temporal correlations also play an important role to feature time series. Here, we follow the most prevalent idea, where RNN is utilized to capture the time correlations. For a window sequence of entity  $k$ ,  $x_k^c$ , the time representation  $H_k^t$  at time  $t \in [cS : cS + T)$  is derived by  $H_k^t = \text{RNN}(x_k^t, H_k^{t-1})$ , where RNN can be any sequence model such as LSTM and GRU [4], and  $H_k^t$  is the hidden state of RNN. To integrate the spatio and temporal information, a graph convolution operation is performed for  $H^t$ . As mentioned in GANF [5], we also find that history information of the node itself helps enhance temporal relationships of time series. Hence, the spatio-temporal condition at time  $t$  is given as:

$$C^t = \text{ReLU}(A^c H^t W_1 + H^{t-1} W_2) W_3 \quad (9)$$

where  $W_1$ ,  $W_2$  are the graph convolution weights and history information weights, respectively.  $W_3$  is used to improve the expression ability of condition representations. The time encoding and spatio-temporal conditions of  $x_k^c$  are obtained as  $H_k^c = \text{Concat}(H_k^{cS}, \dots, H_k^{cS+T-1})$  and  $C_k^c = \text{Concat}(C_k^{cS}, \dots, C_k^{cS+T-1})$  respectively, where  $\text{Concat}(\cdot)$  denotes the concatenation operation.

### 4.5 Entity-aware Normalizing Flow

Distributions of individual entities have discrepancies because of their different work mechanisms, and thus their respective anomalies will generate distinct sparse characteristics. If we map time series from all entities to the same distribution  $N(0, I)$ , as does in GANF, then the description capacity will be largely limited and the unique inherent property of each individual entity will be ignored. Therefore, we design the entity-aware normalizing flow  $z_k = f_{\theta}^k(x|C)$  to make more detailed density estimation, where  $x$ ,  $C$ ,  $k$  are the input sequence, condition and the  $k$ th entity, respectively. Technically, for one entity, we assign the multivariate Gaussian distribution as the target distribution. The covariance matrix of above target distribution is the identity matrix  $I$  for the better convergence. Moreover, in order to generate different target distributions  $\mathcal{Z}_k$ , we independently draw mean vectors  $\mu_k \in \mathcal{R}^T$  from  $N(0, I)$ . However, we find that such setting results in performance degradation. So, in our experiment, each element of  $\mu_k$  is kept the same. Specifically, for the time series of the entity  $k$ , the

density estimation is given by

$$P_{X_k}(x_k) = P_{Z_k}(f_{\theta}^k(x_k|C)) \left| \det \frac{\partial f_{\theta}^k}{\partial x_k^T} \right| \quad (10)$$

$$Z_k = N(\mu_k, I)$$

where each element of  $\mu_k$  is the same, and is drawn from the  $N(0, 1)$ .

In such case, model parameters will increase with the number of entities. To mitigate this problem, we share entity-aware normalizing flow parameters across all entities. So, the density estimation for  $k$  reads

$$P_{X_k}(x_k) = P_{Z_k}(f_{\theta}(x_k|C)) \left| \det \frac{\partial f_{\theta}}{\partial x_k^T} \right| \quad (11)$$

#### 4.6 Joint Optimization

As described above, MTGFlow combines graph structure learning and RNN to capture the spatio and temporal dependence on multiple time series. Then, dervied saptio-temporal conditions are utilized to contribute to entity-aware normalizing flow accurately estimating density of time series. To avoid getting stuck in local optimum for each module of MTGFlow, we jointly optimize all modules for overall performance of MTGFlow. The whole parameters  $W^*$  are estimated via maximum log likelihood.

$$\begin{aligned} W^* &= \arg \max_W \log(P_X(x)) \\ &\approx \arg \max_W \frac{1}{N} \sum_{c=1}^N \frac{1}{K} \sum_{k=1}^K \log(P_{X_k}(x_k^c)) \\ &\approx \arg \max_W \frac{1}{NK} \sum_{c=1}^N \sum_{k=1}^K [\log(P_{Z_k}(f_{\theta}^k(x_k^c|C_k^c))) \left| \det \frac{\partial f_{\theta}}{\partial x_k^c T} \right|] \\ &\approx \arg \max_W \frac{1}{NK} \sum_{c=1}^N \sum_{k=1}^K [-\frac{1}{2} \|\hat{z}_k^c - \mu_k\|_2^2 + \log \left| \det \frac{\partial f_{\theta}}{\partial x_k^c T} \right| + const] \end{aligned} \quad (12)$$

where  $N$  is the total number of windows, and  $const$  is a constant, equal to  $-\frac{T}{2} * \log(2\pi)$ .

#### 4.7 Anomaly Detection and Interpretation

Based on the hypothesis that anomalies tend to be sparse on data distributions, low log likelihoods indicate that the observations are more likely to be anomalous. Taking this advantage, we further extend the above procedure to anomaly detection application and the corresponding interpretation function.

**4.7.1 Anomaly detection.** Taking the window sequence  $x_k^c$  as the input, the density of all entities can be estimated. The mean of the negative log likelihoods of all entities serves as the anomaly score  $S_c$ , which is calculated by:

$$S_c = -\frac{1}{K} \sum_{k=1}^K \log(P_{X_k}(x_k^c)) \quad (13)$$

A higher anomaly score represents that  $x_k^c$  locates in the lower density region, indicating a higher possibility to be abnormal. Since abnormal series exist in training set and validation set, we cannot directly set the threshold to label the anomaly, such as the maximum deviation in validation data [6]. Therefore, to reduce the

anomaly disturbance, we store  $S_c$  of the whole training set, and the interquartile range (IQR) is used to set the anomaly threshold.

$$Threshold = Q_3 + 1.5 * (Q_3 - Q_1) \quad (14)$$

where  $Q_1$  and  $Q_3$  are 25th percentile and the 75th percentile of  $S_c$ .

**4.7.2 Anomaly interpretation.** Abnormal behaviors of any entity could lead to the overall abnormal behaviour of the whole window sequence. Naturally, we can get the entity anomaly score  $S_{ck}$  for entity  $k$  according to Eq. 13

$$S_c = -\frac{1}{K} \sum_{k=1}^K \log(P_{X_k}(x_k^c)) = \sum_{k=1}^K S_{ck} \quad (15)$$

However, we map time series of each entity into unique target distributions, and different ranges of  $S_{ck}$  are observed. This bias will bring each entity plays different weights in contributing to  $S_c$ , which we do not hope. To circumvent the above unexpected bias, we design the entity-specific threshold for each entity. IQR is used to set the respective thresholds, considering different scales of  $S_{ck}$ . Therefore, the threshold for  $S_{ck}$  is given

$$Threshold_k = \lambda_k(Q_3^k + 1.5 * (Q_3^k - Q_1^k)) \quad (16)$$

where  $Q_1^k$  and  $Q_3^k$  are 25th percentile and the 75th percentile of  $S_{ck}$  across all observations, respectively. And  $\lambda_k$  adjusts the  $Threshold_k$  because normal observations of entities also fluctuate with different scales. Moreover, it is possible for an anomaly  $A_i$  to arise from a group of entities (a group anomaly) or just arise from a single anomaly (a point anomaly). To detect the type of the anomaly, we can list the possible causes  $P_k^i$  at  $A_i$ :

$$P_k^i = S_{ck}^i - Threshold_k \text{ for } i, k \in S_{ck}^i > Threshold_k \quad (17)$$

where  $S_{ck}^i$  represents the  $S_{ck}$  at the  $A_i$ . It is assumed that the location at root cause suffers from larger deviation  $P_k^i$ . Therefore, according to the distribution of  $P^i$ , we can tell if a detected anomaly is a group anomaly or a point anomaly.

## 5 EXPERIMENT

### 5.1 Experiment Setup

**5.1.1 Dataset.** The commonly used public datasets for multivariate time series anomaly detection in OCC are SMAP (Soil Moisture Active Passive satellite) [14], MSL (Mars Science Laboratory rover) [14], SMD (Server Machine Dataset) [26], SWaT (Secure Water Treatment) [8] and WADI (Water Distribution). However, the collected time series in SMAP and MSL do not have the same time span and different servers that generate time sequence in SMD are independent. Thereby, it will be inappropriate to employ these three datasets for our comparisons. In the most related previous work GANF [5], SWAT and two private datasets is utilized. Following their setup, we use two public datasets SWaT and WADI in our experiments.

SWaT collects 51 sensor data from a real-world industrial water treatment plant, at the frequency of one second. The dataset provides ground truths of 41 attacks launched during 4 days. WADI collects 121 sensor and actuators data from WADI testbed, at the frequency of one second. The dataset provides ground truths of 15 attacks launched during 2 days. Since only normal time series are

**Table 1: The settings of SWaT and WADI.**

Dataset	Entity	Training/Test set	Anomaly ratio (%)
SWaT	51	269951/89984	17.7/5.2
WADI	123	103680/69121	6.4/4.6

provided in these two datasets for training in OCC setting, we split the original testing dataset by 60% for training, 20% for validation, and 20% for testing in SWaT. As for WADI, the training split contains 60% data, and the test split contains 40% data. The specific statistics are listed in Table 1.

**5.1.2 Implementation details.** For both datasets, we set the window size as 60 and the stride size as 10. Adam optimizer with learning rate 0.002 is utilized to update all parameters. One self-attention layer with 0.2 dropout ratio is adopted to learn the graph structure. We use MAF as the normalizing flow model. For SWaT, we use one flow block and set the batch size as 512. WADI has about twice as many entities as SWaT, we arrange two flow blocks for it and set the batch size as 256.  $\lambda$  is set as 0.8 for thresholds of all entities.

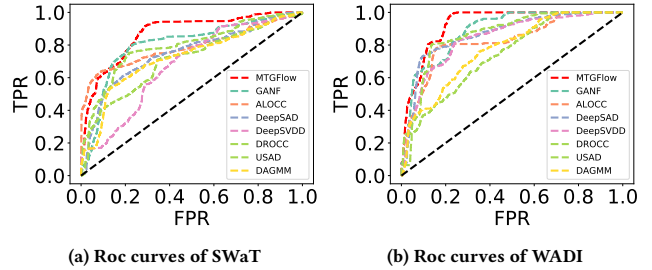
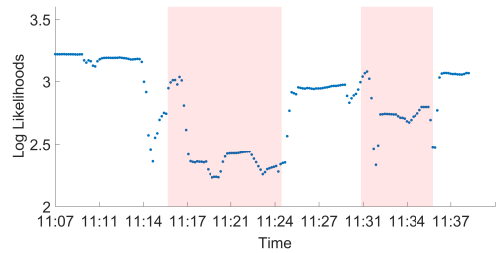
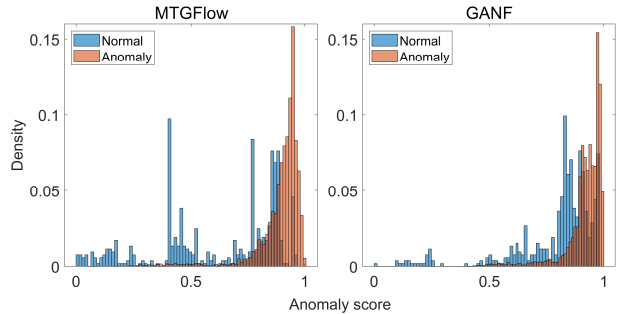
**5.1.3 Evaluation metric.** Following the same setting as the previous works, MTGFlow aims to detect the window-level anomalies. And, the window label is annotated as abnormal when there exists an anomalous time point within the corresponding time duration. We evaluate the performance of MTGFlow on SWaT and WADI by the Area Under the Receiver Operating Characteristic curve (AUROC).

**5.1.4 Baselines.** We compare the SOTA semi-supervised and unsupervised density estimation methods.

- DeepSAD [22]. A semi-supervised method maps normal data into preset hypersphere, and additional anomaly labels are leveraged to improve the detection performance.
- DeepSVDD [21]. An OCC method, maps normal data into preset hypersphere, and anomaly data are assumed to be located outside the hypersphere.
- ALOCC [23]. An OCC method, reconstructs inputs via GAN, and declares anomalies according to the output of the discriminator.
- DROCC [10]. An OCC method, constructs robust representations for normal data. Anomalies will deviate the learned representations.
- USAD [2]. An OCC method, leverages autoencoder to reconstruct inputs. Anomaly data suffer poor reconstruction quality.
- DAGMM [35]. A density estimation approach, combines autoencoder and Gaussian Mixture Model (GMM), the samples with high energy are declared as anomalies.
- GANF [5]. The density estimation approach joints DAG and flow model, and data on low density regions are identified as anomalies.

## 5.2 Performance

As shown in Table 1, SWaT and WADI have the high and low anomaly ratio, respectively. We test MTGFlow in these two datasets to present the performance.

**Figure 2: Comparison with advanced methods son ROC curves for SWaT and WADI.****Figure 3: Log likelihoods for anomalies.****Figure 4: Comparison on normalized anomaly scores between MTGFlow and GANF.**

**5.2.1 Performance on SWaT.** We present the ROC curves in Fig. 2a and list the AUROC metric results in Table 2. MTGFlow has the superior performance over all the other six baselines. Compared with MTGFlow, DeepSVDD and DROCC project all training samples into the hypersphere so that they cannot learn the accurate decision boundary distinguishing normal from abnormal samples. Adversarial learning used by ALOCC and USAD and semi-supervised learning strategy in DeepSAD leverage a more informative training procedure to mitigate the effect of high anomaly contamination. And DAGMM is restricted to the distribution estimation ability of GMM for multiple entities. As GANF obtains a better result, its detection performance is limited to inadequate dependence modeling and indiscriminative density estimation. Our MTGFlow has a much more flexible modeling structure. The dynamic relations among entities and the unique characteristic of each entity can be

**Table 2: Performance of AUROC(%) on SWaT and WADI.**

Dataset	DeepSVDD	ALOCC	DROCC	DeepSAD	USAD	DAGMM	GANF	MTGFlow
SWaT	66.8±2.0	77.1±2.3	72.6±3.8	75.4±2.4	78.8±1.0	72.8 ±3.0	79.8±0.7	<b>84.8±1.5</b>
WADI	83.5±1.6	83.3±1.8	75.6±1.6	85.4±2.7	86.1±0.9	77.2±0.9	90.3±1.0	<b>91.9±1.1</b>

**Table 3: Module ablation study (AUROC%).**

	Graph	Entity-aware	SWaT	WADI
MTGFlow/(G, E)	✗	✗	78.3±0.9	89.7±0.5
MTGFlow/G	✗	✓	82.4±1.0	91.3±0.4
MTGFlow/E	✓	✗	81.2±1.1	91.0±0.7
MTGFlow	✓	✓	<b>84.8±1.5</b>	<b>91.9±1.1</b>

extracted. Profiting from these, MTGFlow accomplishes 84.8% AUROC, outperforming the above mentioned methods. Moreover, we study log likelihoods for anomalies ranging from 2016/1/2 11:07:00 to 11:37:00 in Fig. 3. It is clear that log likelihoods are high for the normal series but lower for labeled abnormal ones (highlight in red). This variation of log likelihoods validates that MTGFlow can detect anomalies according to low density regions of modeled distribution. Meanwhile, to investigate anomaly discrimination ability of MTGFlow, we present the normalized  $S_c$  for MTGFlow and GANF in Fig. 4. As displayed in Fig. 4, for normal series, anomaly scores of MTGFlow are more centered at 0 than these of GANF, and the overlap areas of normal and abnormal scores are also smaller in MTGFlow, reducing the false positive ratio. This larger anomaly score discrepancy corroborates MTGFlow superior anomaly detection performance.

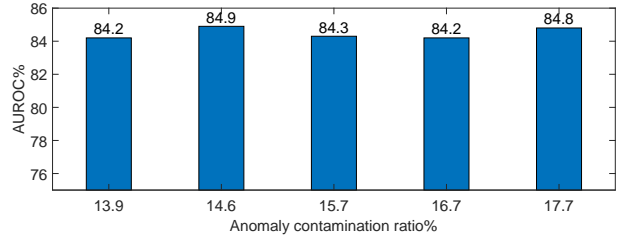
**5.2.2 Performance on WADI.** In the low anomaly ratio scenario, MTGFlow also has a consistently good performance. We show the results in Table 2, where MTGFlow outperforms all other compared methods. However, compared with the substantial advancement in SWaT experiments, MTGFlow achieve a smaller superiority in WADI. From the ROC curves of Fig. 2b, it can be seen that when false positive ration (FPR) is lower than 0.2, there is no obvious difference in the ROC curves. We analyze this phenomenon from AUROC mechanism. When FPR is low, the corresponding anomaly threshold is high. That means time series are all judged to be normal expect for the most obvious anomalies. And coupled with the low anomaly rate, above mentioned drawback of OOC setting is easier to hide, which cannot reflect the true detection ability. Hence, this leads the similar true positive ratio when FPR is below 0.2. With FPR increasing (i.e the threshold is decreasing), more accurate boundary makes TPR of MTGFlow rise rapidly. Conversely, other methods suffer from the unclear boundary between abnormal and normal series and causes slow increase in TPR, thereby widening the anomaly detection performance gap with MTGFlow.

### 5.3 Ablation Study

**5.3.1 Module ablation study.** To test the validity of each designed module, we give several ablation experiments. We denote MTGFlow

**Table 4: Ablation study of hyperparameters (AUROC%)**

Window size	Blocks	1	2	3
SWaT	40	81.4±3.2	82.7±2.1	81.7±0.9
	60	<b>84.8±1.5</b>	83.6±2.0	83.1±0.9
	80	82.8±1.0	82.7±0.8	83.4±0.6
	100	82.6±0.5	83.4±0.9	83.5±0.6
	120	83.2±2.0	83.4±2.3	84.5±2.6
WADI	40	90.8±1.3	91.7±1.2	91.7±1.3
	60	89.2±1.9	<b>91.9±1.1</b>	91.5±0.8
	80	89.8±2.0	90.7±0.8	91.7±0.7
	100	89.6±1.1	90.9±0.8	91.8±0.6
	120	88.6±1.4	91.0±0.6	91.5±0.9

**Figure 5: Effect of anomaly contamination ratio.**

without graph and entity-aware normalizing flow as MTGFlow/(G, E), MTGFlow only without graph as MTGFlow/G, and MTGFlow only without entity-aware normalizing flow as MTGFlow/E. The results are presented in Table 3, where MTGFlow/(G, E) obtains the worst performance. It is attributed to the lack of relational modeling among entities and the indistinguishable density estimation. Applying graph structure learning in model pairwise relations, MTGFlow/E achieves better performance. Also, considering more fine-grained density estimation, MTGFlow/G achieves an improvement over MTGFlow/(G, E). Integrating these two modules, MTGFlow accomplishes the best performance, which demonstrates the effective design of MTGFlow.

**5.3.2 Hyperparameter robustness.** We conduct a comprehensive study for the choice of the hyperparameters, the results are shown in Table 4. Concretely, we conduct experiments with various sizes for the sliding window and three different numbers for the normalizing flow blocks in Table 4. In SWaT, when window size is small, such as 40, 60, and 80, the increase in the number of blocks does not necessarily improve anomaly detection performance. Larger model causes the overfitting to the normal distribution where the abnormal series present in areas of high density. When the window size is large (i.e., 80, 100, and 120), distribution to be estimated is more

high-dimensional so that model needs more capacity. Therefore, detection performance derives average gain with blocks increasing due to more accurate distribution modeling. The analysis can also be applied to WADI dataset. According to the experimental results, 60 for window size and 1 normalizing flow block, and 60 for window size and 2 normalizing flow blocks are the best parameters of MTGFlow on SWaT and WADI, achieving 84.8%, 91.9% AUROC anomaly detection performance, respectively.

**5.3.3 Anomaly ratio analysis.** To further investigate the influence of anomaly contamination rates, we vary training splits to adjust anomalous contamination rates. The training split increases from 60% to 80% with 5% stride, and the corresponding anomaly ratios are 17.7%, 16.7%, 15.7%, 14.6%, and 13.9%, respectively. The test split is 20%. We present an average result over five runs on SWaT in Fig. 5. Although anomaly contamination ratio of training dataset rises, anomaly detection performance of MTGFlow remains at a stable high level, ranging from 84.2% to 84.9%. The robustness to anomaly contamination again confirms the advantage of MTGFlow, using density estimation to detect an anomaly.

## 5.4 Result Analysis

In order to further investigate the effectiveness of MTGFlow, we analyze the obtained results from different aspects on SWaT.

**5.4.1 Dynamic graph structure.** interdependencies among entities are not guaranteed to be immutable. In fact, pairwise relations evolve with time. Benefiting from self-attention, MTGFlow can model this characteristic into a dynamic graph structure. We treat the attention matrix as the graph adjacent matrix. An empirical threshold is set for the adjacency matrix to show an intuitive learned graph structure in test split. In Fig. 6, the node size represents its node degrees, the arrow direction represents the learned directed dependence and the arrow width indicates the weight of the corresponding interdependencies. Graph structure at 2016/1/1 14:00:00 is centered on sensor  $P201$ , while the edges in the graph have completely changed and the center has shifted from  $P201$  to  $AIT503$  at 2016/1/2 7:00:00. This alteration of graph structure may result from changing in working condition of water treatment plant. Therefore, it is necessary to use a dynamic graph to model such changeable interdependencies. Besides, two similar graph structures can be found at 2016/1/2 13:00:00 and 2016/1/2 14:00:00. This suggests that the graph structure will be consistent if the interdependencies remain unchanged over a period of time, possibly due to repetitive work patterns of entities. In addition, the main pairwise relations (thick arrow) at 2016/1/1 14:00:00 is similar as the relations at 2016/1/2 14:00:00, which both centered on  $P201$ . It indicates that the interdependencies on multiple sensors is periodic. We also find mutual interdependencies from learned graph structures, such as the edges between  $P201$  and  $AIT201$  at 2016/1/2 13:00:00 and 2016/1/2 14:00:00. Furthermore, we compare the normalized anomaly score distributions of MTGFlow and MTGFlow/G in Fig. 7 for further analysis of the effectiveness of dynamic graph structure on anomaly detection. Such a dynamic graph design can push anomaly scores of normal series to 0 and enlarge the margin between normal and abnormal series. We summarize the findings: (1) Dynamic interdependencies among multiple entities. (2) Consistent

interdependencies among multiple entities. (3) Periodic interdependencies among multiple entities. (4) Mutual interdependencies among multiple entities.

**5.4.2 Entity-specific density estimation.** We further explore whether distributions of all entities are transformed into different target distributions to verify our entity-aware design. Since the window size is 60, the corresponding transformed distributions are also 60 dimensional distributions. Each single dimension of the multivariate Gaussian distribution is a Gaussian distribution. For a better visualization, we present the 0th dimension of the transformed distributions in Fig. 8. Nine distributions of different entities are displayed. It can be seen that these distributions have been projected as unique distributions. Moreover, these distributions are successfully converted to preset Gaussian distributions with different mean vectors. The one-to-one mapping models entity-specific distributions and captures their respective sparse characteristics of anomalies. Fig. 9 shows the normalized anomaly score distribution for normal and abnormal series. We observe that the margin between normal and abnormal samples in MTGFlow is larger than that in MTGFlow/E. This demonstrates that MTGFlow amplifies the discrepancy between normal and abnormal samples with the help of the entity-specific density estimation.

**5.4.3 Distinct sparse characteristics.** To demonstrate the sparse characteristics vary with different entities, we study changes of  $S_{ck}$  along time on SWaT. As shown in Fig. 10,  $S_{ck}$  of  $AIT201$ ,  $AIT502$ ,  $P102$ ,  $FIT502$ ,  $LIT301$  are presented. The highlighted regions denote marked anomalies. For a better illustration, we divide the anomalous regions as  $A_1$ ,  $A_2$ ,  $A_3$ ,  $A_4$ , and  $A_5$ , alongside the time sequence. It can be observed that  $AIT201$  and  $AIT502$  have obvious fluctuations at  $A_4$ , while  $P102$  reacts to  $A_2$ . Also,  $P403$  is sensitive to  $A_2$  and  $A_4$ ,  $FIT502$  is sensitive to  $A_4$  and  $A_5$ , yet  $LIT310$  is sensitive to  $A_2$ ,  $A_3$ ,  $A_4$ , and  $A_5$ . According to the above results, we valid that different entities present the discrepancy of sparse characteristic.

**5.4.4 Anomaly interpretation.** MTGFlow can also provide the explanation of the detected anomaly via the deviations of their respective  $S_{ck}$ , and tell it is a group anomaly or point anomaly. From Fig. 10, the blue lines are the corresponding thresholds set according to Eq. 16, which considers different scales of individual entities. The value exceeding the thresholds is labeled an abnormal behaviors. In order to further localize the declared anomaly,  $P$  is obtained according to Eq. 17 for all the above mentioned anomalies in Fig. 11. For  $A_1$ ,  $P_3^1$  and  $P_4^1$  are positive and close, so we tend to declare  $A_1$  is a group anomaly occurring at  $P102$  and  $P403$ . Aiming at  $A_2$ , we can observe  $P_2^3$  is much higher than  $P_4^2$  and  $P_6^2$ , in this case the root cause of  $A_2$  is believed that  $P102$  is attacked, and causes the unusual behaviors of  $P102$  and  $LIT301$ . The same analysis can be applied to  $A_3$ ,  $A_4$ , and  $A_5$ .

## 6 CONCLUSION

In this work, we proposed MTGFlow, an unsupervised anomaly detection approach for multivariate time series based on the dataset with absolute zero known labels. Extensive experiments on the real-world datasets demonstrate its superiority, even if there exists high anomaly contamination. MIGFlow achieves 84.8% AUROC on SWaT and 91.9% AUROC on WADI, outperforming SOTA anomaly

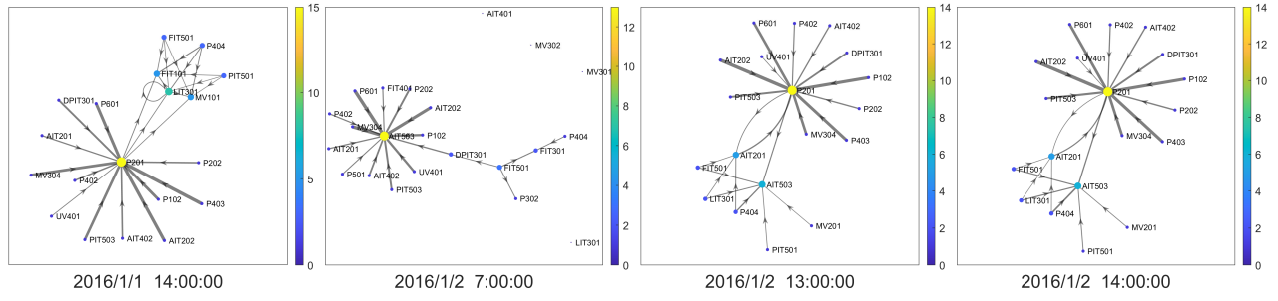


**Figure 6: Dynamic graph structure in MTGFlow.**

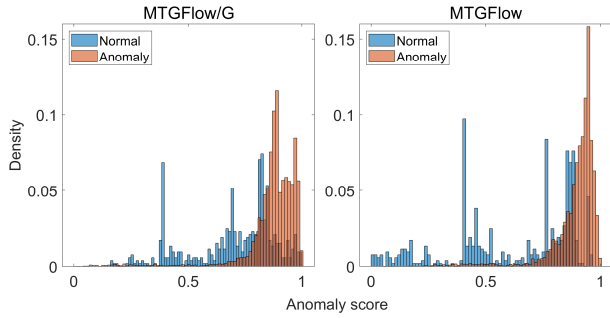


**Figure 7: Comparison on normalized anomaly scores between MTGFlow and MTGFlow/G.**

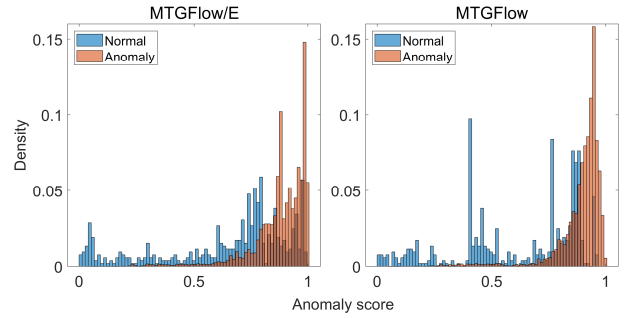


**Figure 9: Comparison on normalized anomaly scores between MTGFlow and MTGFlow/E.**

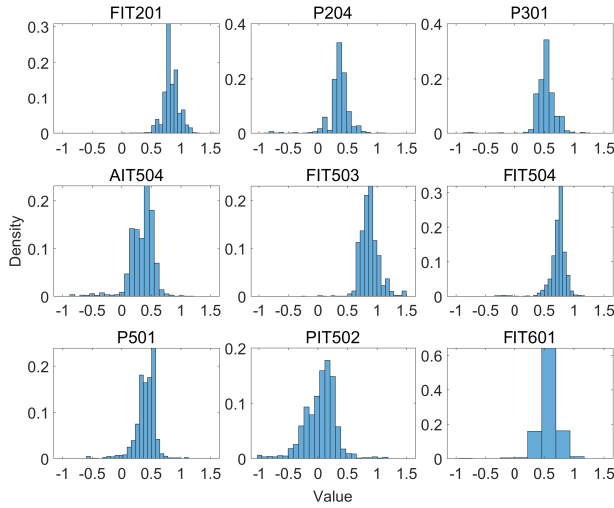


**Figure 8: Transformed distribution of multiple entities.**

plan to apply our model to more flow models and further improve the practicality of our approach.

detection methods. The superior anomaly detection performance of MTGFlow is attributed to dynamic graph structure learning and entity-aware density estimation. In addition, we explore various interdependencies existing among individual entities from the learned dynamic graph structure. And a detected anomaly can be understood and localized via entity anomaly scores. In the future, we

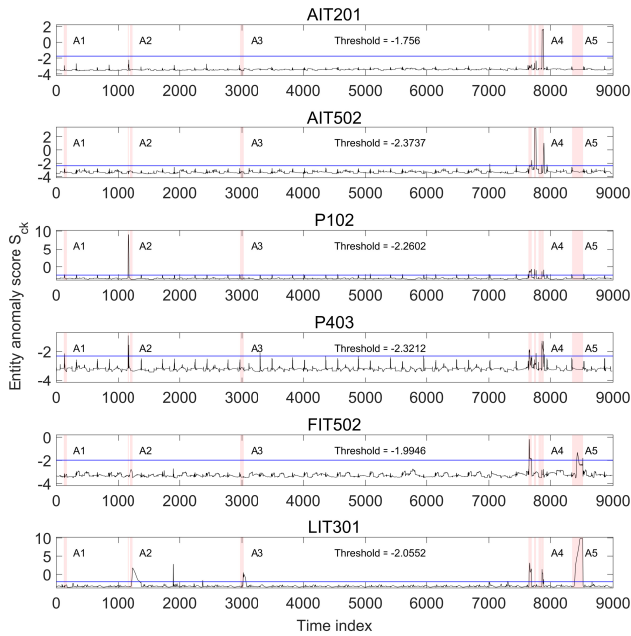


**Figure 10: Variation of Log likelihoods for different entities on the whole testing dataset. Anomaly ground truths are presented as red boxes.**

Entity	$P_1$ (AIT201)	-1.167	-1.028	-1.583	3.42	-1.436
	$P_2$ (AIT502)	-0.4108	-0.2832	-0.8156	5.599	-0.2781
	$P_3$ (P102)	0.1799	11.29	-0.1622	1.609	-0.0991
	$P_4$ (P403)	0.1772	1.412	-0.7715	1.04	-0.2752
	$P_5$ (FIT502)	-1.146	-0.8001	-1.225	1.817	0.6782
	$P_6$ (LIT301)	-0.8561	3.287	2.532	5.194	11.91
		A1	A2	A3	A4	A5
		Anomaly				

**Figure 11: Visualization of the possible causes  $P$ .**

## REFERENCES

- [1] Lynton Ardizzone, Carsten Lüth, Jakob Kruse, Carsten Rother, and Ullrich Köthe. 2019. Guided image generation with conditional invertible neural networks. *arXiv preprint arXiv:1907.02392* (2019).
- [2] Julien Audibert, Pietro Michiardi, Frédéric Guyard, Sébastien Marti, and Maria A Zuluaga. 2020. USAD: unsupervised anomaly detection on multivariate time series. In *Proceedings of the 26th ACM SIGKDD International Conference on Knowledge Discovery & Data Mining*. 3395–3404.
- [3] Xuanhao Chen, Liwei Deng, Feiteng Huang, Chengwei Zhang, Zongquan Zhang, Yan Zhao, and Kai Zheng. 2021. DAEMON: Unsupervised Anomaly Detection and Interpretation for Multivariate Time Series. In *2021 IEEE 37th International Conference on Data Engineering (ICDE)*. IEEE, 2225–2230.
- [4] Kyunghyun Cho, Bart Van Merriënboer, Caglar Gulcehre, Dzmitry Bahdanau, Fethi Bougares, Holger Schwenk, and Yoshua Bengio. 2014. Learning phrase representations using RNN encoder-decoder for statistical machine translation. *arXiv preprint arXiv:1406.1078* (2014).
- [5] Enyan Dai and Jie Chen. 2022. Graph-Augmented Normalizing Flows for Anomaly Detection of Multiple Time Series. *arXiv preprint arXiv:2202.07857* (2022).
- [6] Ailin Deng and Bryan Hooi. 2021. Graph neural network-based anomaly detection in multivariate time series. In *Proceedings of the AAAI Conference on Artificial Intelligence*, Vol. 35. 4027–4035.
- [7] Laurent Dinh, Jascha Sohl-Dickstein, and Samy Bengio. 2016. Density estimation using real nvp. *arXiv preprint arXiv:1605.08803* (2016).
- [8] Jonathan Goh, Sridhar Adepu, Khurum Nazir Junejo, and Aditya Mathur. 2016. A dataset to support research in the design of secure water treatment systems. In *International conference on critical information infrastructures security*. Springer, 88–99.
- [9] Adam Goodge, Bryan Hooi, See Kiong Ng, and Wee Siong Ng. 2021. LUNAR: Unifying Local Outlier Detection Methods via Graph Neural Networks. *arXiv preprint arXiv:2112.05355* (2021).
- [10] Sachin Goyal, Aditi Raghunathan, Moksh Jain, Harsha Vardhan Simhadri, and Prateek Jain. 2020. DROCC: Deep robust one-class classification. In *International Conference on Machine Learning*. PMLR, 3711–3721.
- [11] Denis Gudovskiy, Shun Ishizaka, and Kazuki Kozuka. 2022. Cflow-ad: Real-time unsupervised anomaly detection with localization via conditional normalizing flows. In *Proceedings of the IEEE/CVF Winter Conference on Applications of Computer Vision*. 98–107.
- [12] Manish Gupta, Jing Gao, Charu C Aggarwal, and Jiawei Han. 2013. Outlier detection for temporal data: A survey. *IEEE Transactions on Knowledge and data Engineering* 26, 9 (2013), 2250–2267.
- [13] Sepp Hochreiter and Jürgen Schmidhuber. 1997. Long short-term memory. *Neural computation* 9, 8 (1997), 1735–1780.
- [14] Kyle Hundman, Valentino Constantinou, Christopher Laporte, Ian Colwell, and Tom Soderstrom. 2018. Detecting spacecraft anomalies using lstms and nonparametric dynamic thresholding. In *Proceedings of the 24th ACM SIGKDD international conference on knowledge discovery & data mining*. 387–395.
- [15] Thomas N Kipf and Max Welling. 2016. Semi-supervised classification with graph convolutional networks. *arXiv preprint arXiv:1609.02907* (2016).
- [16] Pankaj Malhotra, Anusha Ramakrishnan, Gaurangi Anand, Lovekesh Vig, Puneet Agarwal, and Gautam Shroff. 2016. LSTM-based encoder-decoder for multi-sensor anomaly detection. *arXiv preprint arXiv:1607.00148* (2016).
- [17] Guansong Pang, Longbing Cao, and Charu Aggarwal. 2021. Deep Learning for Anomaly Detection: Challenges, Methods, and Opportunities. In *Proceedings of the 14th ACM International Conference on Web Search and Data Mining (Virtual Event, Israel) (WSDM '21)*. Association for Computing Machinery, New York, NY, USA, 1127–1130. <https://doi.org/10.1145/3437963.3441659>
- [18] George Papamakarios, Theo Pavlakou, and Iain Murray. 2017. Masked autoregressive flow for density estimation. *Advances in neural information processing systems* 30 (2017).
- [19] Kashif Rasul, Abdul-Saboor Sheikh, Ingmar Schuster, Urs Bergmann, and Roland Vollgraf. 2020. Multivariate probabilistic time series forecasting via conditioned normalizing flows. *arXiv preprint arXiv:2002.06103* (2020).
- [20] Marco Rudolph, Bastian Wandt, and Bodo Rosenhahn. 2021. Same same but different: Semi-supervised defect detection with normalizing flows. In *Proceedings of the IEEE/CVF Winter Conference on Applications of Computer Vision*. 1907–1916.
- [21] Lukas Ruff, Robert Vandermeulen, Nico Goernitz, Lucas Deecke, Shoaib Ahmed Siddiqui, Alexander Binder, Emmanuel Müller, and Marius Kloft. 2018. Deep one-class classification. In *International conference on machine learning*. PMLR, 4393–4402.
- [22] Lukas Ruff, Robert A Vandermeulen, Nico Goernitz, Alexander Binder, Emmanuel Müller, Klaus-Robert Müller, and Marius Kloft. 2019. Deep semi-supervised anomaly detection. *arXiv preprint arXiv:1906.02694* (2019).
- [23] Mohammad Sabokrou, Mahmood Fathy, Guoying Zhao, and Ehsan Adeli. 2020. Deep end-to-end one-class classifier. *IEEE transactions on neural networks and learning systems* 32, 2 (2020), 675–684.
- [24] David Salinas, Valentin Flunkert, Jan Gasthaus, and Tim Januschowski. 2020. DeepAR: Probabilistic forecasting with autoregressive recurrent networks. *International Journal of Forecasting* 36, 3 (2020), 1181–1191.
- [25] Bernhard Schölkopf, Robert C Williamson, Alexander J Smola, John Shawe-Taylor, John C Platt, et al. 1999. Support vector method for novelty detection.. In *NIPS*, Vol. 12. Citeseer, 582–588.
- [26] Ya Su, Youjian Zhao, Chenhao Niu, Rong Liu, Wei Sun, and Dan Pei. 2019. Robust anomaly detection for multivariate time series through stochastic recurrent neural network. In *Proceedings of the 25th ACM SIGKDD international conference on knowledge discovery & data mining*. 2828–2837.
- [27] David M J Tax and Robert PW Duin. 2004. Support vector data description. *Machine learning* 54, 1 (2004), 45–66.
- [28] Shreshth Tuli, Giuliano Casale, and Nicholas R Jennings. 2022. TranAD: Deep Transformer Networks for Anomaly Detection in Multivariate Time Series Data. *arXiv preprint arXiv:2201.07284* (2022).
- [29] Ashish Vaswani, Noam Shazeer, Niki Parmar, Jakob Uszkoreit, Llion Jones, Aidan N Gomez, Łukasz Kaiser, and Illia Polosukhin. 2017. Attention is all you need. *Advances in neural information processing systems* 30 (2017).
- [30] Petar Veličković, Guillem Cucurull, Arantxa Casanova, Adriana Romero, Pietro Lio, and Yoshua Bengio. 2017. Graph attention networks. *arXiv preprint arXiv:1710.10903* (2017).
- [31] Ruoying Wang, Kexin Nie, Yen-Jung Chang, Xinwei Gong, Tie Wang, Yang Yang, and Bo Long. 2020. Deep Learning for Anomaly Detection (KDD '20).

Association for Computing Machinery, New York, NY, USA, 3569–3570. <https://doi.org/10.1145/3394486.3406481>

- [32] Jiehui Xu, Haixu Wu, Jianmin Wang, and Mingsheng Long. 2021. Anomaly Transformer: Time Series Anomaly Detection with Association Discrepancy. *arXiv preprint arXiv:2110.02642* (2021).
- [33] Chiyuan Zhang, Samy Bengio, Moritz Hardt, Benjamin Recht, and Oriol Vinyals. 2021. Understanding deep learning (still) requires rethinking generalization. *Commun. ACM* 64, 3 (2021), 107–115.
- [34] Lingyu Zhang, Jiabao Zhao, and Wei Li. 2019. Online and unsupervised anomaly detection for streaming data using an array of sliding windows and PDDs. *IEEE Transactions on Cybernetics* 51, 4 (2019), 2284–2289.
- [35] Bo Zong, Qi Song, Martin Renqiang Min, Wei Cheng, Cristian Lumezanu, Daeki Cho, and Haifeng Chen. 2018. Deep autoencoding gaussian mixture model for unsupervised anomaly detection. In *International conference on learning representations*.